JCTC Journal of Chemical Theory and Computation

Article

pubs.acs.org/JCTC

Halogen Bonding from Dispersion-Corrected Density-Functional Theory: The Role of Delocalization Error

A. Otero-de-la-Roza,*[,†] Erin R. Johnson,*[,‡] and Gino A. DiLabio*[,§,†]

[†]National Institute for Nanotechnology, National Research Council of Canada, 11421 Saskatchewan Drive, Edmonton, Alberta T6G 2M9, Canada

[‡]Chemistry and Chemical Biology, School of Natural Sciences, University of California, Merced, 5200 North Lake Road, Merced, California 95343, United States

[§]Department of Chemistry, University of British Columbia, Okanagan, Fipke Center 357, 3247 University Way, Kelowna, British Columbia V1V 1V7, Canada

Supporting Information

ABSTRACT: Halogen bonds are formed when a Lewis base interacts with a halogen atom in a different molecule, which acts as an electron acceptor. Due to its charge transfer component, halogen bonding is difficult to model using many common density-functional approximations because they spuriously overstabilize halogen-bonded dimers. It has been suggested that dispersion-corrected density functionals are inadequate to describe halogen bonding. In this work, we show that the exchange-hole dipole moment (XDM) dispersion correction coupled with functionals that minimize delocalization error (for instance, BH&HLYP, but also other half-and-half functionals) accurately model halogen-bonded interactions, with average errors similar to other noncovalent dimers with less charge-transfer effects. The performance of XDM is evaluated for three previously proposed benchmarks (XB18 and XB51 by Kozuch and Martin, and the set proposed by Bauzá et al.) spanning a range of binding energies up to ∼50 kcal/mol. The good performance of BH&HLYP-XDM is comparable to M06-2X, and extends to the "extreme" cases in the Bauzá set. This set contains anionic electron donors where charge transfer occurs even at infinite separation, as well as other charge transfer dimers belonging to the pnictogen and chalcogen bonding classes. We also show that functional delocalization error results in an overly delocalized electron density and exact-exchange hole. We propose intermolecular Bader delocalization indices as an indicator of both the donor−acceptor character of an intermolecular interaction and the delocalization error coming from the underlying functional.

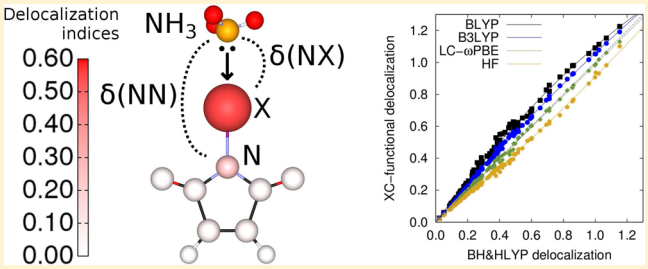

1. INTRODUCTION

Despite its enormous success, density-functional theory (DFT) has a number of well-known shortcomings,[1−4] mostly stemming from the inability of common density functionals to accurately model long-range exchange-correlation effects. Two of these deficiencies are delocalization error and the lack of dispersion interactions.[5,6] In recent years, combining dispersion corrections with pre-existing common functionals (in the following, *base* functionals) has been shown to yield accurate noncovalent binding energies, enabling the use of density-functional theory for the calculation of noncovalent interactions.[6,7] In spite of this success, the application of dispersion corrections still relies heavily on error cancellation, and little attention has been paid to how different base functionals treat the nondispersive part of the intermolecular interaction. In this work, we examine the roles of both the base density-functional approximation and the dispersion correction for the study of halogen-bonded complexes.

Halogen bonding[8−13] is a type of noncovalent interaction that is strongly affected by the choice of base functional. A halogen bond occurs between an electron donor (a lone pair, an electron-rich π-system, etc.) and the so-called σ-hole[10,14] on the halogen atom in the acceptor molecule. The σ-hole is the area of relatively positive charge on the otherwise electronegative halogen atom that arises from the antibonding orbital associated with the Y-halide σ-bond, where Y is the atom to which the halide atom is covalently bonded in the acceptor molecule. Halogen bonds tend to show the strong preference for linearity that is characteristic of intermolecular orbital interactions. This orientation favors maximum overlap between the Y-halide σ^* orbital and the donor lone-pair. Halogen bond strength is proportional to (i) Lewis base strength (electron-donating ability), (ii) polarizability of the acceptor, and (iii) electron-withdrawing strength of groups bonded to the halogen atom accepting the lone pair. Intermolecular orbital interactions are an essential component of halogen bonding, although the extent to which they drive binding compared to electrostatic interactions from accompanying intermolecular charge transfer is debatable.[12,15]

Received: October 8, 2014

   dx.doi.org/10.1021/ct500899h | J. Chem. Theory Comput. XXXX, XXX, XXX−XXX

Halogen-bonded dimers are a type of charge-transfer (CT) complex[15−20] and are therefore affected by delocalization error. Common semilocal density functionals correspond to exchange-correlation hole models that neglect long-range effects. A well-known property relevant for noncovalent interactions[7] is that, as the reference electron moves away from the system, the exchange hole should remain attached to the molecule, a behavior that most density functionals fail to reproduce. In the context of an inter- or intramolecular charge transfer, incorrect long-range hole behavior results in an excessive charge transfer and an attendant overestimation of the binding energy. This is known as delocalization or many-electron self-interaction error;[17,21−23] it arises from approximate density functionals not being linear in the electron density.[17,24] This shortcoming is particularly obvious for systems with fractional charges, whose density is written exactly as a linear combination of densities for integer-electron systems.

Because of delocalization error, semilocal density functionals overestimate the binding energies of CT complexes[16] and the magnitude of fractional charge on each monomer. This behavior has been related to the underestimation of the donor highest occupied molecular orbital (HOMO)-acceptor lowest unoccupied molecular orbital (LUMO) gap.[25,26] The correct description of CT requires the use of either global hybrids with a large fraction of exact exchange equal to or exceeding 50%, or range-separated hybrid functionals with correct long-range asymptotics.[15,26,27] A similar requirement is found for the accurate modeling of charge-transfer excitations in time-dependent DFT.[18,19] The errors associated with charge transfer are present in other noncovalently bonded systems such as radical-molecule complexes,[26,27] anion-molecule complexes,[27] and solvated-electron systems.[28]

Recent articles by Kozuch and Martin[12] and Bauzá et al.[29] stated that dispersion-corrected functionals are unable to represent halogen bonding interactions accurately. In their comprehensive study, Kozuch and Martin[12] observed that common density-functionals overbind systematically, a problem that is aggravated by the application of pairwise dispersion corrections (Grimme's D2[30] and D3[31] in their work), and they speculate that delocalization error is behind this behavior. In consequence, Kozuch and Martin conclude that halogen bonds are "just too complex for simple dispersion corrections" and recommend using alternatives such as M06-2X, which shows excellent performance on standard benchmarks for halogen bonding. In this article, we conclusively demonstrate that delocalization error is behind the spurious overestimation of the halogen-bond strengths by examining a sequence of dispersion-corrected functionals with known delocalization error behavior. In addition, we demonstrate that, provided a functional with low delocalization error is used, a standard pairwise dispersion correction (the exchange-hole dipole moment model, XDM) is able to accurately reproduce the structures and binding energies of halogen-bonded dimers.

A number of qualitative and quantitative descriptors[12,13] and energy partitions[15,32−34] have been used to characterize halogen bonding. In order to evaluate the charge-transfer contribution from different functionals and the role of delocalization error, we use a different approach in this article: intermolecular Bader delocalization indices (DIs). We show that there is a strong correlation between DIs and halogen-bond strengths, regardless of the donor and acceptor character, even for anionic dimers. This correlation is not present when using the donor HOMO−acceptor LUMO gap. We also show that exact exchange-hole delocalization serves as a measure of delocalization error (semilocal functionals predict systematically higher DIs), which decreases as the charge transfer approaches one whole electron in agreement with the known functional behavior for fractional charges.

In this article, we demonstrate two main theses: (i) that dispersion corrections accurately model halogen bonding provided a base functional with low delocalization error is used and (ii) that intermolecular delocalization indices can be used to quantify both the strength of a halogen-bonding interaction and the extent of delocalization error from the base functional.

2. THEORY

In the following, we combine common density-functional approximations in the context of density-functional theory (DFT) with the exchange-hole dipole moment (XDM) model of dispersion.[35,36] XDM is a dispersion correction that allows calculation of the atomic dispersion coefficients without empirical parameters. These coefficients enter an asymptotic pairwise expression for the dispersion energy:

$$E_{\mathrm{XDM}} = -\sum_{n=6,8,10}\sum_{\mathrm{A>B}} C_n^{\mathrm{AB}} R_{\mathrm{AB}}^{-n} f_n(R_{\mathrm{AB}}) \tag{1}$$

where the sum runs over all pairs of atoms, R_{AB} is the interatomic distance, and C_n are the XDM dispersion coefficients. The dispersion energy in eq 1 is added to the energy from the base functional to give the total energy:

$$E_{\mathrm{total}} = E_{\mathrm{base}} + E_{\mathrm{XDM}} \tag{2}$$

The damping function f_n attenuates the dispersion correction at short interatomic distances:[35,37,38]

$$f_n(R_{\mathrm{AB}}) = \frac{R_{\mathrm{AB}}^n}{R_{\mathrm{vdw,AB}}^n + R_{\mathrm{AB}}^n} \tag{3}$$

and contains two adjustable parameters (a_1 and a_2) in $R_{\mathrm{vdw,AB}}$.[37,38] If the base functional gave an exact account of the nondispersive contribution to the total energy, a_1 and a_2 would be physical quantities[7] instead of adjustable parameters, determining the shape of the damping function. In practice, the damping function is used to correct errors from the base functional, such as the delocalization error considered in this article, as well as basis-set incompleteness.[39] The parameters are fitted to the Kannemann−Becke (KB) set,[40,41] which does not contain halogen-bonded or charge transfer dimers. XDM has been shown to perform well for the calculation of noncovalent binding energies in the gas-phase,[7,42] as well as in condensed phases.[43−45]

The other theoretical tool we use in this article is Bader's localization and delocalization indices[46−50] (LIs and DIs), with which we analyze and quantify intermolecular electron delocalization. These indices are defined as integrals of quantities related to the pair density, $\rho(\boldsymbol{r}_1,\boldsymbol{r}_2)$, which gives the probability of finding electrons at $\boldsymbol{r}_1$ and $\boldsymbol{r}_2$. The pair density can be written as

$$\rho(\boldsymbol{r}_1, \boldsymbol{r}_2) = \rho(\boldsymbol{r}_1)\rho(\boldsymbol{r}_2) + \rho_{\mathrm{xc}}(\boldsymbol{r}_1, \boldsymbol{r}_2) \tag{4}$$

where the exchange-correlation density (ρ_{xc}) measures the deviation of the pair density from the independent charge distribution. The exchange-correlation density is integrated in the regions associated with atoms A and B:

dx.doi.org/10.1021/ct500899h | J. Chem. Theory Comput. XXXX, XXX, XXX−XXX

$$F(\mathrm{A},\mathrm{B}) = \int_{\mathrm{A}} \mathrm{d}\boldsymbol{r}_1 \int_{\mathrm{B}} \mathrm{d}\boldsymbol{r}_2 \rho_{\mathrm{xc}}(\boldsymbol{r}_1, \boldsymbol{r}_2) \tag{5}$$

The atomic regions are defined as being encompassed by zero-flux surfaces of the electron density, as in Bader's theory.[51−53] $F(\mathrm{A},\mathrm{B})$ measures the degree of correlation between the electron distributions in both atoms, which we normally refer to as interatomic "delocalization" or "electron sharing". The localization (λ) and delocalization (δ) indices are defined as

$$\lambda(\mathrm{A}) = -F(\mathrm{A},\mathrm{A}) \tag{6}$$

$$\delta(\mathrm{A},\mathrm{B}) = -F(\mathrm{A},\mathrm{B}) - F(\mathrm{B},\mathrm{A}) \tag{7}$$

$\lambda(\mathrm{A})$ measures the number of electrons localized within the basin of atom A and $\delta(\mathrm{A},\mathrm{B})$ is the amount of electron delocalization (sharing) between A and B. The average number of electrons on A ($N(\mathrm{A}) = \int_{\mathrm{A}} \mathrm{d}\boldsymbol{r}\rho(\boldsymbol{r})$) can be partitioned using these indices:

$$N(\mathrm{A}) = \lambda(\mathrm{A}) + \frac{1}{2}\sum_{\mathrm{B}\neq\mathrm{A}} \delta(\mathrm{A},\mathrm{B}) \tag{8}$$

Perfectly localized electrons within atom A have $\lambda(\mathrm{A}) = N(\mathrm{A})$, and $\delta(\mathrm{A},\mathrm{B}) = 0$ for any other atom B. $F(\mathrm{A},\mathrm{B})$ and, consequently, $\delta(\mathrm{A},\mathrm{B})$ and $\lambda(\mathrm{A})$ are invariant with respect to unitary orbital transformations.

The same-spin component of ρ_{xc} embodies the electron correlation effects coming from the antisymmetry requirement of the wave function (Fermi correlation). In the context of wave function theory, Fermi correlation can be calculated exactly at the Hartree−Fock (HF) level. The one-determinant expression for the wave function reduces eq 5 to

$$F(\mathrm{A},\mathrm{B}) = -\sum_{ij} S_{ij}^{\mathrm{A}} S_{ji}^{\mathrm{B}} \tag{9}$$

where S_{ij}^{A} are the atomic overlap matrices:

$$S_{ij}^{\mathrm{A}} = \int_{\mathrm{A}} \mathrm{d}\boldsymbol{r}\psi_i^*(\boldsymbol{r}_1)\psi_j(\boldsymbol{r}_2) \tag{10}$$

and the sum runs over the occupied molecular orbitals ψ_i.

Kohn−Sham DFT uses a monodeterminant representation of noninteracting particles that reproduces the electron density of the system. Hence, eqs 9 and 10 can be applied directly, although the significance of the LIs and DIs differs because the Kohn−Sham pair density (eq 4) has no direct physical interpretation. Instead, δ and λ are quantities that measure the delocalization of the exact exchange hole constructed from the Kohn−Sham orbitals. Models of the exchange hole have been used extensively in DFT as basic objects from which to build exchange-correlation functionals.[54] XDM, for instance, is based on modeling the dipole−dipole interaction between electron exchange-hole pair distributions on different atoms.

We illustrate delocalization error behavior and how it is quantified by DIs using the traditional example[17] of a single electron and two infinitely separated energy wells. If the depth of both wells is the same, symmetry requires that half an electron resides in each. Otherwise, the electron is completely localized in the deepest well with $\delta = 0$. Figure 1 shows the DIs calculated for alkali metal dimer cations, in which two infinitely separated alkali metal atoms share a single valence electron, using several functionals with varying degrees of exact exchange. HF gives $\delta(\mathrm{A},\mathrm{B})$ correctly close to zero, but as the functional incorporates more semilocal character, delocalization error builds up in an almost-exact parabolic shape. Pure functionals predict that the electron is delocalized almost half-and-half between both atoms (charge 0.5, DI 0.5).

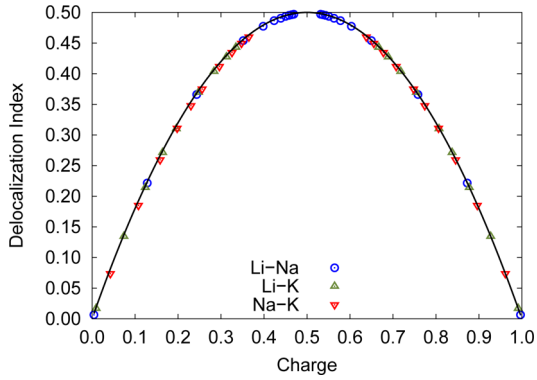

Figure 1. Interatomic delocalization index ($\delta(\mathrm{A},\mathrm{B})$) against Bader charge for three alkali metal dimer cations. The points correspond to different admixtures of exact exchange and B88 exchange. The points closer to the center of the plot (charge = 0.5) have less exact exchange. The black curve is a simple parabola with formula $2x(1 - x)$.

It will be shown in this article that halogen-bonded dimers display similar behavior to that illustrated in Figure 1. Given a noncovalent dimer composed of monomers A and B, we define the intermolecular DI as the sum of all the DIs involving one atom in A and one atom in B.

3. COMPUTATIONAL METHODS

To evaluate the performance of different XDM-corrected functionals, three benchmark sets are used in this article: XB18, XB51, and the Bauzá set. The XB18 and XB51 sets were proposed by Kozuch and Martin[12] and are composed of neutral halogen-bonded dimers. XB18 comprises relatively simple molecules, namely, all combinations between the HCN and OCH_2 electron donors and the following acceptors: HBr, HI, Br_2, I_2, BrI, ClBr, ClI, FBr, and FI. The geometries for these dimers were determined at the CCSD(T)/aug-cc-pVQZ level (in the following, the aug-cc-pVXZ bases[55−57] are represented as aXZ for brevity). The binding energies were obtained by extrapolating CCSD(T) energies calculated using aQZ and a5Z basis sets. The XB51 set is an augmentation of the XB18 set including, in addition to NCH and OCH_2, the PCH and NH_3 donors. The geometries of these were determined at the ωB97XD/aTZ level and the energies were obtained using a composite MP2/CCSD(T) approach.[12]

The set proposed by Bauzá et al.[29] contains rather more "extreme" forms of halogen bonding where anions act as donors. As a result, the binding energies in this set are considerably larger than in XB18 and XB51. This is a good test to explore the limits of extreme delocalization error in functionals and is also relevant for the DFT treatment of electrides[59] and solvated anions. The set also contains dimers featuring chalcogen and pnictogen bonds, which are similar to halogen bonds in that charge transfer is an essential component. The reference data proposed by Bauzá et al. was obtained at the CCSD(T)/aTZ level and presents considerable basis-set superposition error. Consequently, we decided to recalculate the binding energies for all of the halogen-bonded systems in the set using CCSD(T) with the aQZ and a5Z basis sets. The final binding energies were evaluated using Helgaker's two-point extrapolation to the complete basis-set (CBS) limit.[60] As in our previous work,[39,61] half of the counterpoise (CP)

dx.doi.org/10.1021/ct500899h | J. Chem. Theory Comput. XXXX, XXX, XXX−XXX

Table 1. Calculated Binding Energies (kcal/mol) for the Bauzá Set Using CCSD(T) with the Indicated Basis Sets Plus Counterpoise (CP) or Half the Counterpoise Correction[58] (Ave)[a]

name	aQZ	a5Z	CBS	aQZ-CP	a5Z-CP	CBS-CP	Ave-CBS
$Cl^-\cdots ClF$	42.64	43.47	43.97	42.16	43.19	43.85	43.91
$Br^-\cdots ClF$	41.60	42.22	42.63	41.09	41.96	42.59	42.61
$Cl^-\cdots BrF$	45.36	45.93	46.47	44.95	45.69	46.38	46.42
$Br^-\cdots BrF$	42.75	43.20	43.68	42.33	42.98	43.67	43.67
$NH_3\cdots ClF$	11.71	11.99	12.13	11.38	11.82	12.07	12.10
$NH_3\cdots BrF$	15.73	15.86	16.03	15.41	15.71	16.03	16.03
$Cl^-\cdots SF_2$	30.66	31.21	31.56	30.15	30.94	31.49	31.52
$Br^-\cdots SF_2$	25.24	25.56	25.79	24.74	25.35	25.81	25.80
$Cl^-\cdots SeF_2$	40.51	40.91	41.29	39.47	40.08	40.63	40.96
$Br^-\cdots SeF_2$	35.15	35.42	35.72	34.24	34.76	35.28	35.50
$NH_3\cdots SF_2$	7.97	7.96	7.97	7.59	7.83	8.00	7.98
$NH_3\cdots SeF_2$	13.82	13.66	13.57	12.46	12.67	12.89	13.23
$Cl^-\cdots SCF_2$	9.33	9.50	9.56	9.10	9.38	9.52	9.54
$Br^-\cdots SCF_2$	7.63	7.76	7.80	7.43	7.66	7.79	7.80
$Cl^-\cdots SeCF_2$	13.83	13.76	13.70	13.27	13.40	13.52	13.61
$Br^-\cdots SeCF_2$	11.45	11.37	11.29	10.93	11.04	11.15	11.22
$NH_3\cdots SCF_2$	1.73	1.71	1.67	1.61	1.66	1.68	1.67
$NH_3\cdots SeCF_2$	2.87	2.88	2.92	2.52	2.54	2.55	2.73
$Cl^-\cdots SPF_3$	8.35	8.44	8.42	8.11	8.32	8.41	8.42
$Br^-\cdots SPF_3$	6.71	6.78	6.76	6.50	6.68	6.75	6.76
$Cl^-\cdots SePF_3$	15.60	15.60	15.64	15.10	15.16	15.26	15.45
$Br^-\cdots SePF_3$	12.68	12.64	12.64	12.19	12.24	12.31	12.48
$NH_3\cdots SPF_3$	1.49	1.46	1.42	1.37	1.41	1.42	1.42
$NH_3\cdots SePF_3$	3.02	3.02	3.04	2.63	2.63	2.64	2.84
$Cl^-\cdots PF_3$	20.99	21.22	21.41	20.53	20.97	21.33	21.37
$Br^-\cdots PF_3$	15.59	15.65	15.74	15.19	15.47	15.73	15.73
$Cl^-\cdots AsF_3$	34.14	34.30	34.43	33.09	33.61	34.06	34.25
$Br^-\cdots AsF_3$	27.31	27.42	27.54	26.51	26.92	27.31	27.42
$NH_3\cdots PF_3$	5.02	4.88	4.85	4.69	4.77	4.86	4.85
$NH_3\cdots AsF_3$	10.03	9.71	9.45	8.85	9.02	9.18	9.31

[a]The reference data we use in this work is the last column (Ave-CBS).

correction was included since the full counterpoise correction tends to overcompensate for basis-set incompleteness effects.[58,60,62,63] Note, however, that the CP correction is relatively small because of the large size of the basis sets we employed. The CCSD(T) calculations were all performed using the Turbomole program.[64] The results are shown in Table 1. The geometries of all dimers in the Bauzá set are given in the Supporting Information.

Binding energies for all of the halogen-bonding complexes were computed with Gaussian09[65] for selected functionals using the aTZ (which is already close to the basis-set limit[39] for DFT-based methods) and the aQZ basis sets. The difference between both basis sets in terms of mean average errors (MAE) for the three benchmark sets is around or less than 0.1 kcal/mol regardless of the functional. In the rest of the article, we report only the aQZ results except where explicitly stated. Binding energy calculations at the equilibrium geometry were carried out by relaxing the geometry at the aTZ level and then running a single point calculation at the final geometry using aQZ. Relativistic effects have been shown to be important for halogen-bonding energies and geometries,[12] so we introduced those using the aug-cc-pVTZ-PP and aug-cc-pVQZ-PP pseudopotential and basis-set combinations[66−68] for the Br, I, and Pd atoms.

We show in the next section that delocalization error is almost exclusively determined by the fraction of exact exchange in the functional. Several popular exchange-correlation functionals were chosen to explore the role of delocalization error with fractions of exact exchange ranging from 0% to 50%. Three generalized-gradient approximation (GGA) functionals (BLYP,[69,70] PBE,[71] and PW86PBE[71,72]), three hybrid functionals (B3LYP,[70,73] PBE0,[74] BH&HLYP[75]) and three range-separated functionals (CAM-B3LYP[76] and LC-ωPBE[77,78] with two choices of range-separation parameter, ω = 0.2 and 0.4) were used. In particular instances where we examine in detail the effect of the exact exchange component, we use hybrids built using combinations of exact exchange and the BLYP,[69,70] PBE,[71] PW86PBE,[71,72] and TPSS[79] semilocal functionals. These hybrids are composed of exact exchange (x fraction) complemented with the semilocal exchange functional ($1 - x$) and the correlation functional.

XDM dispersion energies were computed using the postg program,[7,80] and damping parameters for use with each base functional were taken from previous work.[7] Calculations with the M06-2X functional,[81] without XDM, were also performed for comparison. Analysis of the Bader DIs was performed using the aimall program.[82] The DIs were calculated using the aug-cc-pVTZ basis sets.

4. RESULTS AND DISCUSSION

4.1. Delocalization Error and Intermolecular Charge Transfer. We first examine the effect of delocalization error on the binding energies of halogen-bonded dimers by plotting the electronic energy (E) as a function of donor−acceptor charge

dx.doi.org/10.1021/ct500899h | J. Chem. Theory Comput. XXXX, XXX, XXX−XXX

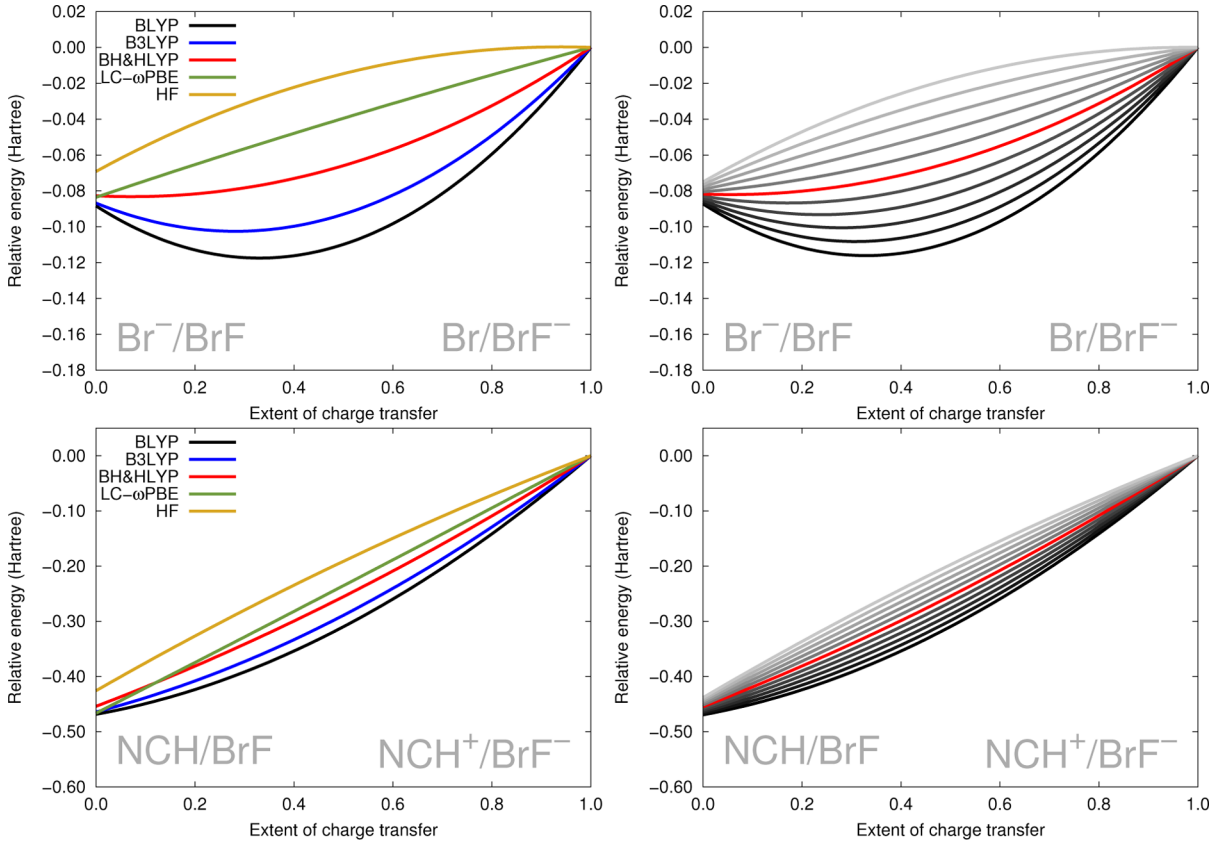

Figure 2. Energy versus fractional charge transfer plots for selected complexes at infinite separation: $Br^-\cdots BrF$ (top) and NCH···BrF (bottom). The zero of energy for each complex has been set as the energy of the right-hand side complex. The plots on the left show the fractional charge behavior for several popular functionals. The plots on the right correspond to PBE with various fractions of exact exchange using a grayscale. The scale goes from 0% (black) to 100% (light gray) in steps of 10%. The red curve corresponds to 50%.

transfer[26,28] at infinite separation. Figure 2 shows a plot of this quantity for two representative halogen-bonded complexes. The plots are obtained using the energies of the neutral molecules and ions, as well as their frontier orbital energies. Let us use the $Br^-\cdots BrF$ dimer as an illustrative example. For each of the two monomers (Br^- and BrF), we generate the fractional charge plot that corresponds to the charge transfer process in the dimer. Because Br^- is the electron donor, we consider the $Br^- \rightarrow Br$ process, and BrF is the electron acceptor, so we plot $BrF \rightarrow BrF^-$. In both cases, the energy versus fractional charge q is written as a cubic spline:[28]

$$E(q) = (\Delta E)q + [(\varepsilon_0 - \Delta E)\,(1 - q) + (\Delta E - \varepsilon_1)q]q(1 - q) \quad (11)$$

where ΔE is the energy difference between the species with $N + 1$ and N electrons, ε_0 is the LUMO eigenvalue of the species with N electrons and ε_1 is the HOMO energy of the species with $N + 1$ electrons. The $E(q)$ of the separated monomers are then added to give the energy as a function of the extent of intermolecular charge transfer within the dimer.

The exact functional should give energies that are piecewise linear functions, with derivative discontinuities at integer electron numbers.[83] Therefore, the energy as a function of charge transfer should also be linear, with the minimum energy point corresponding to the situation where the charge is fully localized on the monomer with the greatest electron affinity. Instead of correctly giving straight lines, GGA functionals deviate from linearity owing to the overstabilization of fractional charges. For hybrid functionals, as the amount of exact exchange increases, the convexity of the fractional energy decreases, and the curves become linear for a fraction around 50%, although this value depends on the system. If the exact exchange component increases past that value, the fractional energy curve becomes concave, resulting in spurious localization ("localization error").

It is important to note that the delocalization error behavior of GGA and hybrid functionals is almost exclusively dependent on the fraction of exact exchange in their composition. Figure 2 shows that BLYP (semilocal), B3LYP (20% exact exchange), and BH&HLYP (50%) have almost exactly the same fractional charge behavior as the corresponding PBE-based hybrids. The same coincidence can be observed if one uses other semilocal functionals as a base for the hybrids, for instance, PW86PBE, BLYP, or TPSS. The corresponding figures can be found in the Supporting Information.

In the particular case of halogen bonding, there are essentially two fractional charge behavior regimes, as exemplified by $Br^-\cdots BrF$ and NCH···BrF in Figure 2. The former category contains dimers with extremely good electron donors, such as the anionic dimers in the Bauzá set. At their equilibrium geometries, these dimers present higher charge transfer and binding energies than the neutral dimers. The defining characteristic is that the HOMO of the donor is higher in energy than the LUMO of the acceptor, and as a consequence, charge transfer occurs even when the monomers are infinitely separated, a case similar to our previous results for a solvated-electron model system.[28] Even at infinite separation,

dx.doi.org/10.1021/ct500899h | J. Chem. Theory Comput. XXXX, XXX, XXX−XXX

Table 2. Mean Absolute Errors (MAE) and Mean Errors (ME) for the XB18, XB51, and Bauzá et al. Benchmark Sets Using the Selected Functionals[a]

	XB18						XB51				Bauzá et al.			
	base		XDM		opt.		base		XDM		base		XDM	
functional	MAE	ME	MAE	ME	MAE	ME	MAE	ME	MAE	ME	MAE	ME	MAE	ME
PBE	0.89	0.75	1.56	1.56	1.74	1.74	1.29	0.80	1.77	1.76	2.56	2.22	3.24	3.19
PW86PBE	0.76	0.61	1.45	1.45	1.51	1.48	1.10	0.56	1.54	1.52	1.97	1.13	2.22	1.96
BLYP	0.90	−0.81	1.17	1.17	1.17	1.17	1.44	−0.97	1.18	1.14	1.85	−1.02	1.68	0.92
PBE0	0.54	−0.38	0.49	0.41	0.68	0.67	0.83	−0.06	0.92	0.89	1.70	1.48	2.44	2.43
B3LYP	1.11	−1.11	0.39	0.34	0.54	0.54	1.22	−1.02	0.62	0.58	1.32	−0.63	1.18	0.96
BH&HLYP	1.52	−1.52	0.35	−0.34	0.21	0.17	1.33	−1.33	0.29	0.06	1.15	−0.97	0.67	0.66
M06-2X	0.24	−0.11			0.21	0.15	0.33	0.07			0.93	0.88		
LC-ωPBE ω = 0.2	0.65	−0.50	0.47	0.42	0.49	0.41	0.89	−0.56	0.61	0.48	1.32	−0.09	1.15	0.85
LC-ωPBE ω = 0.4	1.41	−1.41	0.66	−0.66	0.66	−0.66	1.33	−1.32	0.61	−0.49	1.42	−1.19	0.95	−0.53
CAM-B3LYP	0.74	−0.73	0.35	0.25	0.35	0.25	0.90	−0.79	0.50	0.37	1.12	−0.63	0.70	0.65

[a]Results are shown for both the base and XDM-corrected functionals at the reference geometries. The "Opt." column indicates that the geometries were optimized using the XDM-corrected functional.

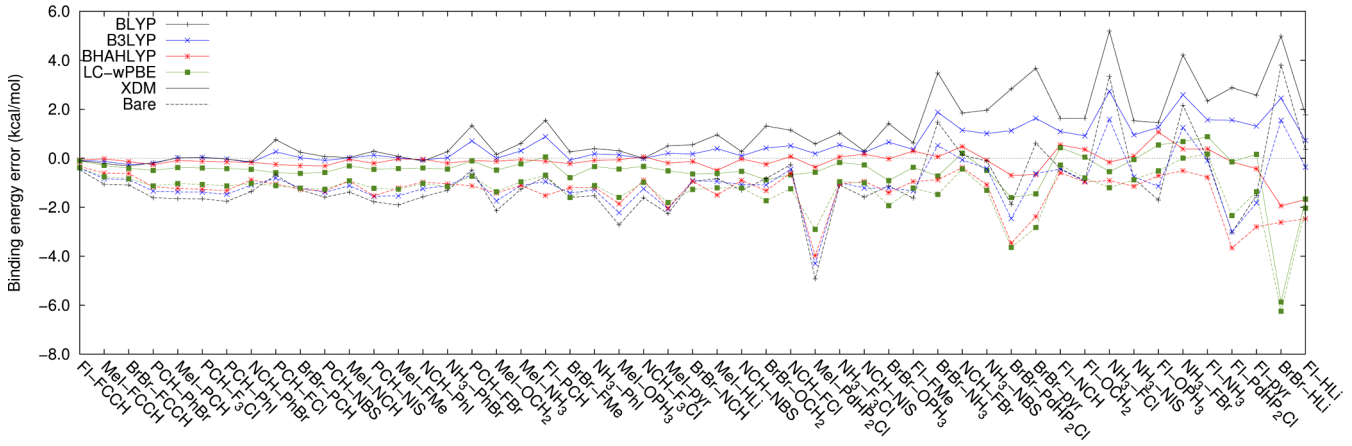

Figure 3. Binding energy errors for the XB51 set with a selected set of functionals. Dashed lines correspond to the base functionals and solid lines to the XDM dispersion-corrected functionals. The dimers have been ordered from left to right by increasing reference binding energy.

GGA functionals predict a density where the electrons are shared between the monomers, with a charge transfer corresponding to the minimum in Figure 2.

The fractional charge plots for the neutral halogen-bonded dimers look like the NCH···BrF example in Figure 2. These dimers present lower charge transfer at the equilibrium geometry and lower binding energies. The plot shows that there is no charge transfer at infinite separation because the donor HOMO is lower in energy than the acceptor LUMO. In this case, all functionals, even GGAs, give a better description, with a small curvature and no minimum at fractional charges. Hence, for charge transfer to occur, the monomers need to approach each other such that the donor HOMO engages in an orbital interaction with the acceptor LUMO.

It is unlikely that the failings of GGA functionals for the calculation of binding energies of neutral halogen-bonded complexes come from self-interaction error in the monomers, as suggested by Steinmann et al.[15] in the more general context of charge-transfer complexes. Many-electron self-interaction error is apparent in systems with fractional charges, and those only occur at the dimer geometry. Also, indicators of charge transfer behavior for neutral dimers based on the isolated monomers, such as the donor HOMO-acceptor LUMO gap[26] or the monomer electrostatic potential[14] are limited for the description of halogen bonds, because of the dramatic change in electronic structure upon dimer formation.

Delocalization error in the dimer and the resulting overstabilization of fractional charges explains the overbinding tendency of GGA functionals for halogen bonds and the results in the following section. Since GGA functionals spuriously overbind the complexes, addition of a dispersion correction, which will further increase the binding, degrades the results, as noted by Kozuch and Martin.[12] B3LYP also gives $E(q)$ plots with significant curvature, but LC-ωPBE and BH&HLYP are more nearly linear and consequently give the lowest binding-energy errors when paired with XDM dispersion. LC-ωPBE with the default range-separation parameter (ω = 0.4) actually gives the opposite curvature, characteristic of the "localization error" seen in HF theory, and thus underestimates both the degree of charge transfer and the binding in these complexes.

4.2. Benchmark of Dispersion-Corrected Functionals.

The mean errors (ME) and mean absolute errors (MAE) for all functionals considered on the three benchmark sets are reported in Table 2. In these results, we used the dimer geometries at which the reference data was calculated (except for the XB18 "opt." data, for which the geometries were relaxed). A representative plot showing the binding energy errors for the individual dimers in the XB51 set is given in Figure 3. A detailed list of all binding energy values obtained

dx.doi.org/10.1021/ct500899h | J. Chem. Theory Comput. XXXX, XXX, XXX−XXX

and plots showing the binding energy errors for the dimers in the other two benchmark sets can be found in the Supporting Information.

Table 2 shows that, on average, the PBE and PW86PBE functionals overbind and BLYP underbinds halogen-bonded complexes in all three sets. The MAEs are slightly under 1 kcal/mol for the XB18 set, slightly larger than 1 kcal/mol for the XB51, and close to 2 kcal/mol in the Bauzá set, with small differences between the three GGA functionals. The MEs for the three GGAs follow the known behavior of their respective exchange functionals in representing the Pauli repulsive wall between closed-shell systems. Namely, PW86PBE gives repulsive energies between closed-shell systems comparable to HF (the correct result) whereas PBE is overly attractive and BLYP is too repulsive.[40,43] Correspondingly, the MEs for the XB18 show that PBE overbinds by 0.75 kcal/mol, PW86PBE overbinds less than PBE (0.61 kcal/mol), and BLYP underbinds by 0.81 kcal/mol. The same trend is present in the other sets.

When the XDM dispersion correction is applied, all GGA functionals overbind. This suggests that, while erroneous Pauli repulsive behavior at the base functional level can be corrected by parametrizing the damping function, errors coming from delocalization error can not. Incorporating dimers with sizable orbital interactions in the parametrization set would only degrade the performance of the dispersion-corrected functional in dimers where the binding energy has a lesser charge-transfer component.

Regarding the hybrid functionals, the performance of XDM-corrected functionals improves with increasing exact exchange, which is a typical indication of delocalization error.[26] Let us consider BLYP, B3LYP (20% exact exchange), and BH&HLYP (50% exact exchange), which form a sequence with decreasing delocalization error (see previous section), and the XB18 set. The unadorned functionals are, on average, overly repulsive, and the MEs increase in absolute value with the amount of exact exchange (−0.81 kcal/mol for BLYP, −1.11 for B3LYP, and −1.52 for BH&HLYP). In contrast, the corresponding dispersion-corrected functionals are overbinding for BLYP and B3LYP, and underbinding for BH&HLYP. The MAE is larger for BLYP-XDM (1.17 kcal/mol) than for B3LYP-XDM (0.39 kcal/mol) and BH&HLYP-XDM (0.35 kcal/mol). B3LYP-XDM gives a MAE almost as low as BH&HLYP for the XB18, but not for the XB51 and Bauzá sets, and the MAE for the XB18 with relaxed geometries is also better in BH&HLYP. This points to a fortuitous error cancellation in the particular case of B3LYP-XDM on XB18.

BH&HLYP-XDM, which has the lowest delocalization error of all three functionals discussed above, is relatively accurate on average. The MAE on the XB18 is slightly larger than M06-2X (0.22 kcal/mol), but comparable to the average errors obtained for other noncovalent interactions using the same functional. For instance, the MAEs in Table 2 are 0.35 (XB18), 0.29 (XB51), and 0.67 (Bauzá) kcal/mol, comparable to the MAEs for other sets lacking charge transfer complexes: 0.28 (KB set[41]), 0.47 (S22[84]), and 0.31 (S66[85]) kcal/mol.[7] The same cannot be said for B3LYP (XB18:0.39, XB51:0.62, Bauzá:1.18, and KB:0.23, S22:0.31, S66:0.22 kcal/mol[7]) or BLYP (XB18:1.17, XB51:1.18, Bauzá:1.68, and KB:0.27, S22:0.22, S66:0.19 kcal/mol[7]).

These observations are analogous to those for hydrogen-atom transfer barriers,[7] and point to the presence of delocalization error. Consequently, while the base functionals alone give reasonably accurate results in some cases, they rely on error cancellation between delocalization error and neglect of dispersion interactions, and their use is not recommended.[12] The same trends are observed for the other sets (XB51 and Bauzá) and for the PBE/PBE0 pair. We note that the statistics for B3LYP-XDM and PBE0-XDM on the XB18 and XB51 are similar to those reported by Kozuch and Martin[12] using the D2[30] and D3[31] dispersion corrections. Specifically, the MAEs for XB18 are 0.64 (B3LYP-D3), 0.22 (B3LYP-D2), 0.62 (PBE0-D3), and 0.36 (PBE0-D2) kcal/mol to be compared to 0.39 (B3LYP-XDM) and 0.49 (PBE0-XDM) kcal/mol. The MAEs for XB51 reported by Kozuch et al. are 0.92 (B3LYP-D3), 0.54 (B3LYP-D2), 0.98 (PBE0-D3), and 0.74 (PBE0-D2), similar to those reported in Table 2: 0.62 (B3LYP-XDM) and 0.92 (PBE0-XDM) kcal/mol. This indicates that trouble with base-functional delocalization error is also present when using other dispersion corrections.

From Table 2, XDM-corrected range-separated functionals give improved performance with respect to GGA-XDM functionals, but the results are sensitive to the range-separation parameter. Range-separated functionals use a semilocal exchange functional to describe electron−electron interactions at short distances, and exact exchange at long-range. The range-separation parameter (ω) controls the onset of the short and long-range regimes. The $\omega \to 0$ and $\omega \to \infty$ limits correspond to the semilocal exchange functional and exact exchange, respectively. CAM-B3LYP has 65% long-range exact exchange and ω = 0.33, whereas LC-ωPBE has 100% long-range exact exchange and ω = 0.4. Table 2 shows that LC-ωPBE-XDM with ω = 0.2 overbinds on average (for the XB18, MAE = 0.47 kcal/mol, ME = 0.42 kcal/mol), while LC-ωPBE-XDM with ω = 0.4 underbinds (MAE = 0.66 kcal/mol, ME = −0.66 kcal/mol). The optimal ω for bare LC-ωPBE seems to be between 0.2 and 0.4 in these systems. However, the optimal range-separation parameter depends on the system size,[86] which limits the applicability of tuning the ω according to these results.

BH&HLYP-XDM and M06-2X give the best performance when the three sets are considered, with the lowest mean absolute errors (MAEs) and mean errors (MEs) near zero. In particular, BH&HLYP-XDM performs well even for the more pathological cases in the Bauzá set, where there is a great deal of charge transfer between the monomers, as well as for the chalcogen and pnictogen-bonded dimers. The performance of M06-2X for the XB51 (MAE[86] 0.33 kcal/mol) and particularly for the Bauzá set (MAE[86] 0.93 kcal/mol) is not as good as BH&HLYP-XDM. The latter is probably caused by the dimers in the Bauzá set being chemically further from the M06-2X parametrization set than those in the XB18 and the XB51 sets.

As stated before, the low BH&HLYP-XDM MAEs are significant because the XDM parametrization set does not contain systems with as much charge transfer as halogen-bonded dimers. Despite this, BH&HLYP-XDM attains performance for the halogen-bonded dimers comparable to other systems containing only hydrogen-bonded and dispersion-dominated dimers, which present far less charge-transfer behavior. By using a base functional that is relatively free from delocalization error, such as BH&HLYP, the XDM dispersion correction yields binding energies with errors that are not different on average from other noncovalent interactions with a lesser charge transfer component. As we will see, the same effect can be observed for hybrids constructed using other semilocal functionals. The average errors for the

dx.doi.org/10.1021/ct500899h | J. Chem. Theory Comput. XXXX, XXX, XXX−XXX

halogen-bonding set are only comparable to the parametrization set when the amount of exact exchange in the functional is close to 50%, regardless of the semilocal functional employed.

In order to further confirm the role of delocalization error in the overbinding behavior of dispersion-corrected GGA functionals, we consider now a collection of hybrid functionals built using the BLYP, PW86PBE, PBE, and TPSS functionals, and fractions of exact exchange from 0% to 100% in 10% steps. The MAEs of these functionals for the XB18 are shown in Table 3.

Table 3. Mean Absolute Error (MAE, in kcal/mol) of Hybrid Functionals Built Using the BLYP, PW86PBE, PBE, TPSS Semilocal Functionals, and the Amount of Exact Exchange Given in the %EXX Column for the XB18 Halogen-Bonding Benchmark Set[12] (Described in the Text) and the 49-Dimer Kannemann−Becke Set Used for the XDM Parametrization[40,41]

	BLYP		PW86PBE		PBE		TPSS	
%EXX	XB18	KB	XB18	KB	XB18	KB	XB18	KB
0	1.20	0.28	1.37	0.39	1.56	0.48	1.26	0.36
10	0.74	0.23	1.03	0.34	1.02	0.43	0.82	0.33
20	0.38	0.21	0.50	0.33	0.64	0.40	0.53	0.31
30	0.38	0.21	0.82	0.33	0.77	0.39	0.74	0.30
40	0.23	0.25	0.36	0.34	0.35	0.39	0.42	0.31
50	0.35	0.31	0.53	0.38	0.48	0.42	0.61	0.33
60	0.49	0.40	0.76	0.42	0.70	0.45	0.82	0.38
70	0.59	0.51	0.96	0.48	0.90	0.50	1.05	0.43
80	0.65	0.64	1.14	0.55	1.10	0.56	1.24	0.50
90	0.68	0.77	1.28	0.63	1.26	0.63	1.40	0.58
100	0.69	0.92	1.40	0.71	1.40	0.71	1.53	0.66

For every hybrid, we determined the damping function parameters by fitting to the Kanemann-Becke set[40,43] (KB), which is the usual procedure in XDM. The KB set does not contain halogen-bonded or charge transfer complexes. The corresponding dispersion-corrected functionals are then applied to the XB18 halogen-bonded set. We can see in Table 3 that all pure GGA functionals show very large errors, corresponding to a strong overestimation of the dimer binding energies. As the amount of exact exchange increases, the MAE decreases, and it reaches a minimum between 40% and 50%, regardless of the semilocal functional used. The adequacy of a given semilocal functional naturally depends on other considerations such as the position of the Pauli repulsive wall,[7,40] but it is only at or around 50% exact exchange that halogen-bonded dimers are treated at the same accuracy level as other noncovalent dimers where charge-transfer effects are a less important contribution to the total binding energy.

Figure 4 shows the effect of building functionals with increasing fractions of exact exchange using BLYP and PBE as the semilocal components on a particular halogen-bonded dimer (the linear complex NCH···FI). All BLYP-based hybrids underbind with respect to the reference. B88, the exchange component of BLYP, is repulsive compared to HF, so when the fraction of exact exchange increases there is a cancellation of effects between decreasing delocalization error and less Pauli repulsion. Despite this, the former dominates in the 0% to 50% range: the hybrid becomes less binding and the equilibrium distance increases as the amount of exact exchange increases. The same effect is observed in the 0% to 50% curves for PBE, although in this case the exchange component becomes more repulsive with increasing exact exchange fraction, leading to a more marked displacement of the dissociation curves. Past the 50% fraction, localization error sets in and binding increases again.

The global effect of the dispersion correction is to shift all curves down by an amount that is small relative to the binding energies from the base functional. In the case of BLYP, the agreement with the reference distance and binding energy for the half-and-half dispersion-corrected functional is almost perfect. Even though the result for unadorned BLYP is also quite good, the statistics in Table 3 show that the result for this particular dimer is not generalizable, whereas the good performance of the half-and-half functional is consistent across the entire benchmark set. PBE underestimates the equilibrium distance with or without dispersion correction, and the dispersion-corrected half-and-half PBE hybrid slightly overestimates the binding energy. This is not surprising given that unadorned PBE considerably understimates Pauli repulsion relative to BLYP[7] and therefore the performance for other noncovalent interactions is worse (MAE = 0.48 kcal/mol on the KB set) compared to BLYP (0.28 kcal/mol). Despite this, Table 3 shows that it is only the half-and-half PBE functional that consistently achieves a good performance for all dimers in the XB18 set, comparable to the MAE statistics for the parametrization set.

Therefore, we can conclude that the overbinding behavior observed in halogen-bonded and other charge-transfer dimers is caused by delocalization error, and should be corrected at the base functional level, and it is not the dispersion correction that is responsible for this failure, as suggested before.[12,29] It is significant that BH&HLYP has also been proposed as a functional with very low self-interaction error in the context of charge-transfer excitations,[19] and that M06-2X (which performs well for dispersion-dominated and charge-transfer dimers) contains a similar amount of exact exchange (54%).

To conclude, we consider the ability of our chosen functionals to model the dimer geometries and the binding energies upon relaxation using the reference geometries for the XB18 set, which were calculated at the CCSD(T) level. Table 4 shows the errors in the calculated donor−acceptor atom−atom distances for all dimers in the XB18 set. The behavior of the distance MAEs is somewhat parallel to that of the geometry-relaxed binding energies in Table 2. The error is larger for GGA functionals, decreases for the PBE0 and B3LYP hybrids, and is virtually zero for BH&HLYP and small for M06-2X. This is reassuring because, even though they are of critical importance, geometries are not used in XDM parametrizations. The table shows that, by minimizing delocalization error at the base functional level, the geometries of halogen-bonded dimers are more accurately represented.

4.3. Intermolecular Delocalization Indices. Given the impact that delocalization error has on noncovalent binding energies, and the likelihood that it affects any noncovalent interaction in which CT is important, we aim to develop a quantitative indicator for charge transfer and delocalization error effects. To be useful, this index should (i) correlate with the total binding energy, (ii) be sensitive to functional delocalization error, and (iii) be valid for any donor−acceptor combination. The index should be based on the overlapping dimer, rather than the isolated monomers. The reason is that, in constrast to the dimer at its equilibrium geometry, there is no charge transfer between infinitely separated monomers (see Section 4.1).

dx.doi.org/10.1021/ct500899h | J. Chem. Theory Comput. XXXX, XXX, XXX−XXX

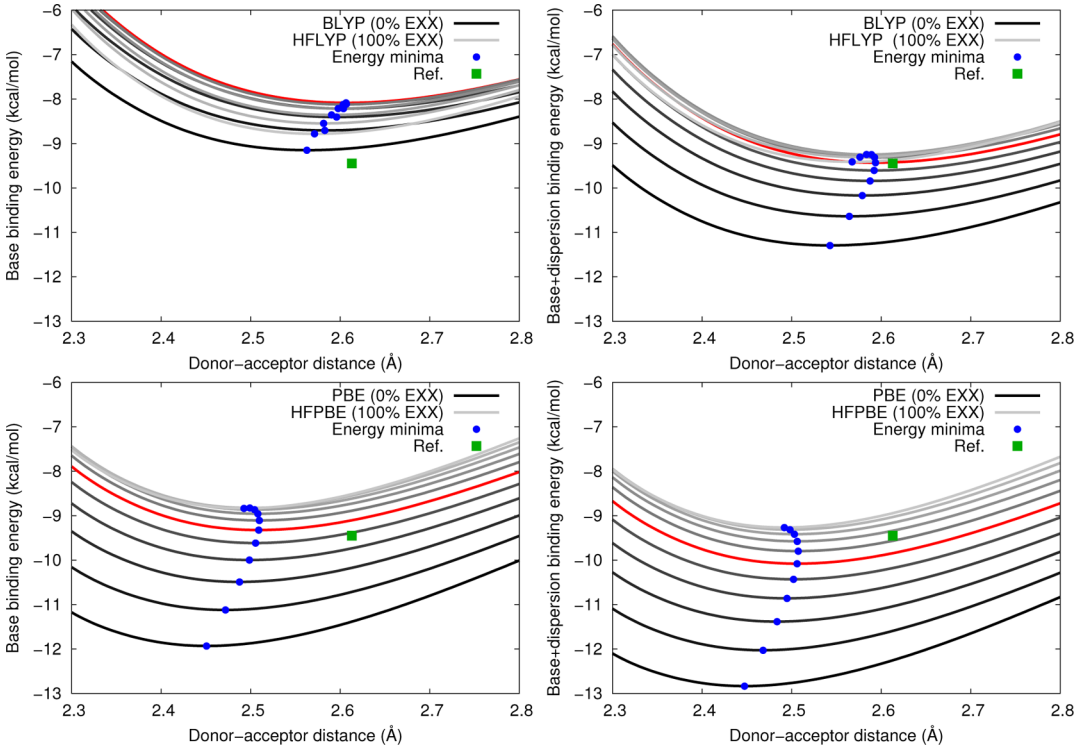

Figure 4. Dissociation energy curves (in kcal/mol) for the linear NCH···FI complex using hybrids built on the BLYP (top) and PBE (bottom) semilocal functionals. The plots on the left show the curves for the base functional alone, and the plots on the right show the results for the corresponding dispersion-corrected functionals. The abscissa gives the distance between the donor (N) and the acceptor (I) atoms, in Å. In each plot, the black curve represents the pure GGA functional and the lightest gray is HF plus the corresponding correlation functional. The grayscale represents intermediate fractions in 10% steps, with a lighter color corresponding to a higher percentage of exact exchange. The 50% exact exchange functional is represented by the red curve. For every energy curve, the minimum is marked with a blue dot. The green square represents the reference (CCSD(T)) distance and binding energy.

Table 4. Mean Absolute Error (MAE) and Mean Error (ME) in the Calculated Intermolecular Distances for Different Functionals and the XB18 Set[a]

	MAE	ME
PBE	0.135	−0.135
PW86PBE	0.104	−0.090
BLYP	0.095	−0.095
PBE0	0.082	−0.078
B3LYP	0.050	−0.049
BH&HLYP	0.006	0.001
M06-2X	0.020	−0.002
LC-ωPBE ω = 0.2	0.070	−0.058
LC-ωPBE ω = 0.4	0.038	0.011
CAM-B3LYP	0.038	−0.038

[a]All functionals are XDM-corrected except M06-2X. The intermolecular distance is taken as the distance between the donor and the acceptor atom. All units are angstrom.

The most obvious indicator of CT is the amount of density that transfers from the donor to the acceptor at the dimer geometry, as measured by population analysis techniques. We have studied two possibilities: Hirshfeld[87] and Bader[51] atomic partitionings. Based on data for the XB18 set, the extent of charge transfer is heavily dependent on the choice of atomic partitioning and, more importantly, the correlation of the charge transfer with the binding energies is poor. Conversely, the DI for the halogen-bonded dimers in Figure 5 correlate well with the reference binding energies, suggesting that the binding in these systems is better described in terms of orbital interactions and electron sharing rather than charge transfer. In addition to correlating with the binding energies, the DIs are also sensitive to delocalization error and functionals with increased delocalization error give higher DI values. BH&HLYP and LC-ωPBE, which have less delocalization error, give the lowest DIs of all the functionals, and the strongest correlation with the reference binding energies (linear for NCH, slightly concave for OCH_2). Hartree−Fock, which is known to be affected by localization error, underestimates the DIs compared to BH&HLYP.

Figure 6 shows a plot of the DIs from all functionals against those of BH&HLYP for the dimers in all three benchmark sets. The spread is found to be largest at intermediate DI values and, as integer values are approached, which corresponds to an almost-complete charge transfer situation in the anionic dimers, delocalization error decreases. The curvature and the deviation from BH&HLYP increases with the amount of delocalization error from the functional, in a remarkable parallel with the fractional charge plots in Section 4.1 (Figure 2). Hartree−Fock shows the characteristic localization error and curves downward, in a convex shape. This result is reasonable because, as indicated before, delocalization error is more important for fractional charge situations. The spread of DIs for functionals with varying amounts of exact exchange can be used as indicator for delocalization error.

Lastly, we consider whether there is a universal correlation between intermolecular DIs and binding energies in halogen bonding. A correlation between binding energy and distance has been recently reported by Tawfik and Donald.[88] In

dx.doi.org/10.1021/ct500899h | J. Chem. Theory Comput. XXXX, XXX, XXX−XXX

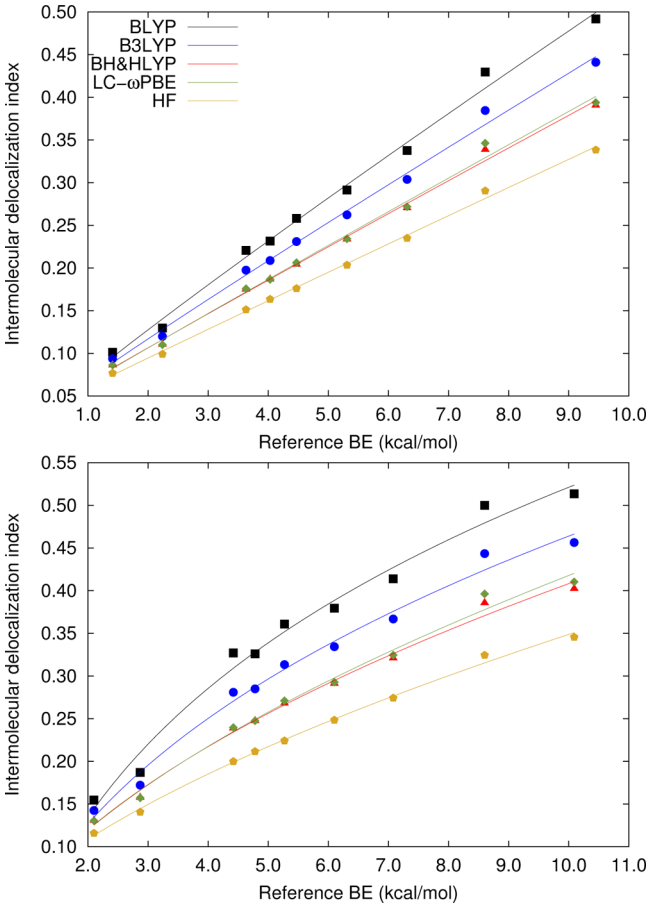

Figure 5. Intermolecular Bader delocalization indices as a function of reference binding energies (kcal/mol) for the XB18 set with selected functionals. The top panel represents the data for the dimers with the NCH donor, and the dimers with the OCH_2 donor are represented in the bottom panel.

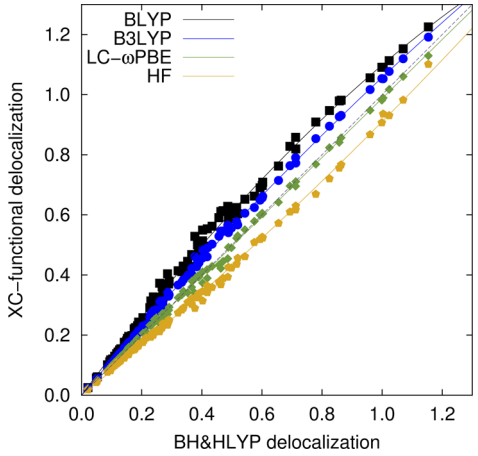

Figure 6. Intermolecular delocalization index computed using selected functionals versus the BH&HLYP values for the XB18, XB51, and Bauzá sets.

Figure 7, we plot the BH&HLYP DIs against the reference binding energies for the three benchmark sets. A correlation between DIs and binding energies is clear and mostly independent of the donor and acceptor identity. The results can be fit to a function of the form $\delta = a\mathrm{BE}^n$ with $a = 0.0987$ and $n = 0.6123$. There are two outliers: all complexes with PCH

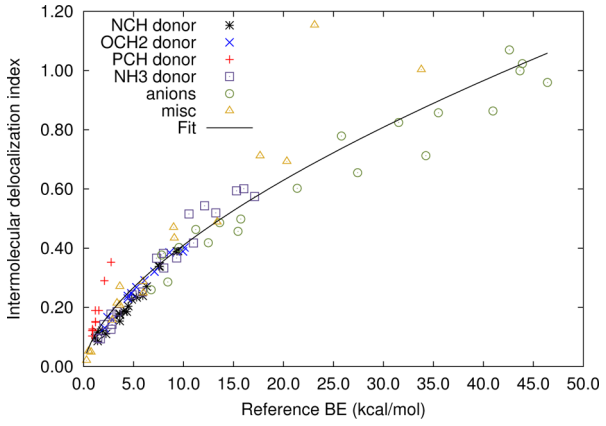

Figure 7. Intermolecular delocalization index computed using BH&HLYP as a function of the reference binding energies for all of the halogen-bonded complexes (XB18, XB51, and Bauzá sets). Different donors are represented by different colors and symbols.

donors and the Br_2—H···Li dimer. The PCH donor curve has a steeper slope probably because of the larger size of the P atom. More delocalization is needed to achieve a given binding energy because the acceptor is farther away from the donor. Br_2—H···Li (from the miscellaneous set in Figure 6, at BE around 23 kcal/mol and 1.10 DI) is an outlier because the structure of this dimer is more correctly represented as Br···Br—H···Li, with a H···Br distance of only 1.63 Å (to be compared to the covalent distance in the HBr molecule, 1.42 Å). Although further study is required, the DIs seem to be a reliable descriptor of halogen bonding.

5. CONCLUSIONS

In this article, we have shown that a pairwise dispersion correction (the exchange-hole dipole moment model, XDM) can be used for modeling halogen bonds provided the base functional gives a correct description of the nondispersive part of the interaction. In particular, we have demonstrated that halogen bonding is greatly affected by delocalization error from the base functional, which is particularly severe in semilocal functionals, and results in a gross overestimation of the binding energy when the dispersion correction is applied. However, if the delocalization error in the base functional is minimized, XDM obtains high accuracy for halogen bonding, similar to that achieved for other noncovalent interactions with less charge transfer. In particular, by using hybrid functionals with 50% exact exchange, the average error in the calculation of halogen-bonded binding energies is similar to other noncovalent dimers with less or no charge transfer effects. This observation applies regardless of the semilocal functional used to build the hybrid functional.

By studying three benchmark sets comprising halogen-bonded dimers (XB18, XB51) as well as more general charge transfer complexes (Bauzá et al.), we have shown that BH&HLYP-XDM in particular gives excellent binding energies for halogen-bonded systems, with average errors comparable to those obtained for noncovalent dimers with far less charge transfer, and similar to M06-2X. In contrast to M06-2X, however, the good performance also extends to cases with extreme charge transfer, such as the anionic dimers proposed by Bauzá et al., which may have relevance in the modeling of noncovalent anionic systems in density-functional theory.

dx.doi.org/10.1021/ct500899h | J. Chem. Theory Comput. XXXX, XXX, XXX–XXX

In addition, we have shown that intermolecular delocalization indices, as defined in Bader's theory, provide a quantitative measure of intermolecular orbital interactions in halogen bonding. Intermolecular DIs display an excellent correlation with the binding energies of halogen-bonded dimers, even at the very high values obtained for the anionic dimers. The intermolecular delocalization indices are also sensitive to delocalization error from the base functional: the spread in DI values for the same dimer using functionals with varying amounts of exact exchange can be used as a measure of delocalization error. Although more study is required, we are confident that the ability of DIs to detect delocalization error will translate to other intermolecular interactions, such as hydrogen bonds, where the intermolecular charge transfer component is not negligible.

■ ASSOCIATED CONTENT

Supporting Information

Geometries of all dimers in the Bauzá set, detailed list of all binding energy values obtained, plots showing the binding energy errors for the dimers in the XB51 and Bauzá sets, fractional charge plots for two selected halogen-bonded dimers and a collection of hybrid functionals, and intermolecular charge transfer plots for the XB18 using Hirshfeld and Bader atomic partitions. This material is available free of charge via the Internet at http://pubs.acs.org.

■ AUTHOR INFORMATION

Corresponding Authors

*E-mail: alberto.oterodelaroza@nrc-cnrc.gc.ca.
*E-mail: ejohnson29@ucmerced.edu.
*E-mail: gino.dilabio@ubc.ca.

Notes

The authors declare no competing financial interest.

■ ACKNOWLEDGMENTS

A.O.R. thanks the Spanish Malta/Consolider initiative (no. CSD2007-00045). G.A.D. thanks a special computing resource allocation and nanoAlberta for financial support. We thank Westgrid for allocation of computing resources.

■ REFERENCES

(1) Cohen, A. J.; Mori-Sánchez, P.; Yang, W. *Science* **2008**, *321*, 792.
(2) Cohen, A. J.; Mori-Sánchez, P.; Yang, W. *Chem. Rev.* **2011**, *112*, 289.
(3) Burke, K. *J. Chem. Phys.* **2012**, *136*, 150901.
(4) Becke, A. D. *J. Chem. Phys.* **2014**, *140*, 18A301.
(5) Johnson, E. R.; Mackie, I. D.; DiLabio, G. A. *J. Phys. Org. Chem.* **2009**, *22*, 1127.
(6) DiLabio, G. A.; Otero-de-la Roza, A. *Rev. Comp. Chem.* **2014**, *arXiv*, 1405.1771.
(7) Otero-de-la Roza, A.; Johnson, E. R. *J. Chem. Phys.* **2013**, *138*, 204109.
(8) Lommerse, J. P. M.; Stone, A. J.; Taylor, R.; Allen, F. H. *J. Am. Chem. Soc.* **1996**, *118*, 3108−3116.
(9) Metrangelo, P.; Neukirch, H.; Pilati, T.; Resnati, G. *Acc. Chem. Res.* **2005**, *38*, 386−395.
(10) Politzer, P.; Murray, J. S.; Clark, T. *Phys. Chem. Chem. Phys.* **2010**, *12*, 77487757.
(11) Rezac, J.; Riley, K. E.; Hobza, P. *J. Chem. Theory Comput.* **2012**, *8*, 4285−4292.
(12) Kozuch, S.; Martin, J. M. L. *J. Chem. Theory Comput.* **2013**, *9*, 1918−1931.
(13) Pinter, B.; Nagels, N.; Herrebout, W. A.; De Proft, F. *Chem. Phys. Phys. Chem.* **2013**, *19*, 519−530.
(14) Clark, T.; Hennemann, M.; Murray, J. S.; Politzer, P. *J. Mol. Model.* **2007**, *13*, 291−296.
(15) Steinmann, S. N.; Piemontesi, C.; Delacht, A.; Corminboeuf, C. *J. Chem. Theory Comput.* **2012**, *8*, 1629−1640.
(16) Ruiz, E.; Salahub, D. R.; Vela, A. *J. Chem. Phys.* **1996**, *100*, 12265−12276.
(17) Zhang, Y. K.; Yang, W. T. *J. Chem. Phys.* **1998**, *109*, 2604−2608.
(18) Tozer, D. J. *J. Chem. Phys.* **2003**, *119*, 12697−12699.
(19) Dreuw, A.; Weisman, J. L.; Head-Gordon, M. *J. Chem. Phys.* **2003**, *119*, 2943−2946.
(20) Ruzsinszky, A.; Perdew, J. P.; Csonka, G. I.; Vydrov, O. A.; Scuseria, G. E. *J. Chem. Phys.* **2006**, *125*, 194112.
(21) Perdew, J. P.; Zunger, A. *Phys. Rev. B* **1981**, *23*, 5048.
(22) Mori-Sánchez, P.; Cohen, A. J.; Yang, W. *J. Chem. Phys.* **2006**, *125*, 201102.
(23) Johnson, E. R.; Mori-Sánchez, P.; Cohen, A. J.; Yang, W. *J. Chem. Phys.* **2008**, *129*, 204112.
(24) Yang, W.; Zhang, Y.; Ayers, P. W. *Phys. Rev. Lett.* **2000**, *84*, 5172.
(25) Sini, G.; Sears, J. S.; Bredas, J. L. *J. Chem. Theory Comput.* **2011**, *7*, 602609.
(26) Johnson, E. R.; Salamone, M.; Bietti, M.; DiLabio, G. A. *J. Phys. Chem. A* **2013**, *117*, 947−952.
(27) Smith, J. M.; Alahmadi, Y. J.; Rowley, C. N. *J. Chem. Theory Comput.* **2013**, *9*, 4860−4865.
(28) Johnson, E. R.; Otero-de-la Roza, A.; Dale, S. G. *J. Chem. Phys.* **2013**, *139*, 184116.
(29) Bauzá, A.; Alkorta, I.; Frontera, A.; Elguero, J. *J. Chem. Theory Comput.* **2013**, *9*, 5201−5210.
(30) Grimme, S. *J. Comput. Chem.* **2006**, *27*, 1787−1799.
(31) Grimme, S.; Antony, J.; Ehrlich, S.; Krieg, H. *J. Chem. Phys.* **2010**, *132*, 154104.
(32) Riley, K. E.; Hobza, P. *J. Chem. Theory Comput.* **2008**, *4*, 232−242.
(33) Wolters, L. P.; Bickelhaupt, F. M. *ChemistryOpen* **2012**, *1*, 96−105.
(34) Wang, C.; Danovich, D.; Mo, Y.; Shaik, S. *J. Chem. Theory Comput.* **2014**, *10*, 3726−3737.
(35) Becke, A. D.; Johnson, E. R. *J. Chem. Phys.* **2005**, *122*, 154104.
(36) Becke, A. D.; Johnson, E. R. *J. Chem. Phys.* **2007**, *127*, 154108.
(37) Johnson, E. R.; Becke, A. D. *J. Chem. Phys.* **2005**, *123*, 024101.
(38) Johnson, E. R.; Becke, A. D. *J. Chem. Phys.* **2006**, *124*, 174104.
(39) Johnson, E. R.; Otero-de-la Roza, A.; Dale, S. G.; DiLabio, G. A. *J. Chem. Phys.* **2013**, *139*, 214109.
(40) Kannemann, F. O.; Becke, A. D. *J. Chem. Theory Comput.* **2009**, *5*, 719−727.
(41) Kannemann, F. O.; Becke, A. D. *J. Chem. Theory Comput.* **2010**, *6*, 1081−1088.
(42) Otero-de-la Roza, A.; Mallory, J. D.; Johnson, E. R. *J. Chem. Phys.* **2014**, *140*, 18A504.
(43) Otero-de-la Roza, A.; Johnson, E. R. *J. Chem. Phys.* **2012**, *136*, 174109.
(44) Otero-de-la Roza, A.; Johnson, E. R. *J. Chem. Phys.* **2012**, *137*, 054103.
(45) Otero-de-la Roza, A.; Cao, B. H.; Price, I. K.; Hein, J. E.; Johnson, E. R. *Angew. Chem., Int. Ed.* **2014**, *53*, 7879−7882.
(46) Bader, R.; Stephens, M. *J. Am. Chem. Soc.* **1975**, *97*, 7391−7399.
(47) Fulton, R. L. *J. Phys. Chem.* **1993**, *97*, 7516−7529.
(48) Bader, R. F.; Streitwieser, A.; Neuhaus, A.; Laidig, K. E.; Speers, P. *J. Am. Chem. Soc.* **1996**, *118*, 4959−4965.
(49) Fradera, X.; Austen, M. A.; Bader, R. F. *J. Phys. Chem. A* **1999**, *103*, 304−314.
(50) Fradera, X.; Poater, J.; Simon, S.; Duran, M.; Solà, M. *Theor. Chem. Acc.* **2002**, *108*, 214−224.
(51) Bader, R. F. W. *Atoms in Molecules. A Quantum Theory*; Oxford University Press: Oxford, 1990.
(52) Bader, R. F. W. *Chem. Rev.* **1991**, *91*, 893−928.

(53) Boyd, R.; Matta, C. *The Quantum Theory of Atoms in Molecules: From Solid State to DNA and Drug Design*; Wiley-VCH: Weinheim, Germany, 2007.
(54) Becke, A.; Roussel, M. *Phys. Rev. A* **1989**, *39*, 3761.
(55) Dunning, T., Jr. *J. Chem. Phys.* **1989**, *90*, 1007.
(56) Kendall, R. A.; Thom, H.; Dunning, J.; Harrison, R. J. *J. Chem. Phys.* **1992**, *96*, 6796−6806.
(57) Woon, D. E.; Thom H. Dunning, J. *J. Chem. Phys.* **1993**, *98*, 1358−1371.
(58) DiLabio, G. A.; Johnson, E. R.; Otero-de-la Roza, A. *Phys. Chem. Chem. Phys.* **2013**, *15*, 12821−12828.
(59) Dale, S. G.; Otero-de-la Roza, A.; Johnson, E. R. *Phys. Chem. Chem. Phys.* **2014**, *16*, 14548−14593.
(60) Halkier, A.; Klopper, W.; Helgaker, T.; Jorgensen, P.; Taylor, P. R. *J. Chem. Phys.* **1999**, *111*, 9157−9167.
(61) Mackie, I. A.; DiLabio, G. A. *J. Chem. Phys.* **2011**, *135*, 134318.
(62) Liedl, K. R. *J. Chem. Phys.* **1998**, *108*, 3199−3204.
(63) Dunning, T. H., Jr. *J. Phys. Chem. A* **2000**, *104*, 9062−9080.
(64) *TURBOMOLE*, V6.5, 2013; a development of University of Karlsruhe and Forschungszentrum Karlsruhe GmbH, 1989−2007, TURBOMOLE GmbH, since 2007; available from http://www.turbomole.com.
(65) Frisch, M. J.; Trucks, G. W.; Schlegel, H. B.; Scuseria, G. E.; Robb, M. A.; Cheeseman, J. R.; Scalmani, G.; Barone, V.; Mennucci, B.; Petersson, G. A.; Nakatsuji, H.; Caricato, M.; Li, X.; Hratchian, H. P.; Izmaylov, A. F.; Bloino, J.; Zheng, G.; Sonnenberg, J. L.; Hada, M.; Ehara, M.; Toyota, K.; Fukuda, R.; Hasegawa, J.; Ishida, M.; Nakajima, T.; Honda, Y.; Kitao, O.; Nakai, H.; Vreven, T.; Montgomery, J. A., Jr.; Peralta, J. E.; Ogliaro, F.; Bearpark, M.; Heyd, J. J.; Brothers, E.; Kudin, K. N.; Staroverov, V. N.; Kobayashi, R.; Normand, J.; Raghavachari, K.; Rendell, A.; Burant, J. C.; Iyengar, S. S.; Tomasi, J.; Cossi, M.; Rega, N.; Millam, J. M.; Klene, M.; Knox, J. E.; Cross, J. B.; Bakken, V.; Adamo, C.; Jaramillo, J.; Gomperts, R.; Stratmann, R. E.; Yazyev, O.; Austin, A. J.; Cammi, R.; Pomelli, C.; Ochterski, J. W.; Martin, R. L.; Morokuma, K.; Zakrzewski, V. G.; Voth, G. A.; Salvador, P.; Dannenberg, J. J.; Dapprich, S.; Daniels, A. D.; Farkas, Ã.; Foresman, J. B.; Ortiz, J. V.; Cioslowski, J.; Fox, D. J. *Gaussian 09*, Revision A.1; Gaussian Inc.: Wallingford, CT, 2009.
(66) Peterson, K. A. *J. Chem. Phys.* **2003**, *119*, 11099−11112.
(67) Peterson, K. A.; Puzzarini, C. *Theor. Chem. Acc.* **2005**, *114*, 283−296.
(68) Peterson, K. A.; Shepler, B. C.; Figgen, D.; Stoll, H. *J. Phys. Chem. A* **2006**, *110*, 13877−13883.
(69) Becke, A. D. *Phys. Rev. A* **1988**, *38*, 3098−3100.
(70) Lee, C.; Yang, W.; Parr, R. G. *Phys. Rev. B* **1988**, *37*, 785−789.
(71) Perdew, J.; Burke, K.; Ernzerhof, M. *Phys. Rev. Lett.* **1996**, *77*, 3865−3868.
(72) Perdew, J. P.; Wang, Y. *Phys. Rev. B* **1986**, *33*, 8800.
(73) Becke, A. D. *J. Chem. Phys.* **1993**, *98*, 5648−5652.
(74) Adamo, C.; Barone, V. *J. Chem. Phys.* **1999**, *110*, 6158−6170.
(75) Becke, A. *J. Chem. Phys.* **1993**, *98*, 1372.
(76) Yanai, T.; Tew, D. P.; Handy, N. C. *Chem. Phys. Lett.* **2004**, *393*, 51−57.
(77) Vydrov, O. A.; Scuseria, G. E. *J. Chem. Phys.* **2006**, *125*, 234109.
(78) Vydrov, O. A.; Heyd, J.; Krukau, A. V.; Scuseria, G. E. *J. Chem. Phys.* **2006**, *125*, 074106.
(79) Tao, J.; Perdew, J. P.; Staroverov, V. N.; Scuseria, G. E. *Phys. Rev. Lett.* **2003**, *91*, 146401.
(80) See http://gatsby.ucmerced.edu/wiki/.
(81) Zhao, Y.; Truhlar, D. G. *Theor. Chem. Acc.* **2008**, *120*, 215241.
(82) Keith, T. A. *AIMAll*, Version 14.06.21; TK Gristmill Software: Overland Park, KS, 2014 (aim.tkgristmill.com).
(83) Perdew, J. P.; Parr, R. G.; Levy, M.; Balduz, J. L. *Phys. Rev. Lett.* **1982**, *49*, 1691−1694.
(84) Jurečka, P.; Šponer, J.; Černỳ, J.; Hobza, P. *Phys. Chem. Chem. Phys.* **2006**, *8*, 1985−1993.
(85) Rezac, J.; Riley, K. E.; Hobza, P. *J. Chem. Theory Comput.* **2011**, *7*, 2427−2438.
(86) Koerzdoerfer, T.; Sears, J. S.; Sutton, C.; Bredas, J. L. *J. Chem. Phys.* **2011**, *135*, 204107.
(87) Hirshfeld, F. L. *Theor. Chim. Acta* **1977**, *44*, 129−138.
(88) Tawfik, M.; Donald, K. J. *J. Phys. Chem. A* **2014**, *118*, 10090−10100.